World Academy of Science, Engineering and Technology
International Journal of Mechanical and Mechatronics Engineering
Vol:10, No:8, 2016

A Detection Method of Faults in Railway Pantographs Based on Dynamic Phase Plots

G. Santamato, M. Solazzi, A. Frisoli

***Abstract*—**Systems for detection of damages in railway pantographs effectively reduce the cost of maintenance and improve time scheduling. In this paper, we present an approach to design a monitoring tool fitting strong customer requirements such as portability and ease of use. Pantograph has been modeled to estimate its dynamical properties, since no data are available. With the aim to focus on suspensions health, a two Degrees of Freedom (DOF) scheme has been adopted. Parameters have been calculated by means of analytical dynamics. A Finite Element Method (FEM) modal analysis verified the former model with an acceptable error. The detection strategy seeks phase-plots topology alteration, induced by defects. In order to test the suitability of the method, leakage in the dashpot was simulated on the lumped model. Results are interesting because changes in phase plots are more appreciable than frequency-shift. Further calculations as well as experimental tests will support future developments of this smart strategy.

***Keywords*—**Pantograph models, phase-plots, structural health monitoring, vibration-based condition monitoring.

I. Introduction

CONDITION monitoring plays a key-role in the maintenance cycle of both civil and mechanical structures; the identification of incipient damages before breakdown is an effective way to achieve predictive safety as well to get economic benefit and, more generally, to improve the quality of service.

Damage detection may be implemented to identify faults in terms of: i) existence; ii) location; iii) severity and furthermore to estimate the residual service life [1].

Almost all the industrial world is concerned with this theme, and also railway industry is pointing towards intensive research. In the last twenty years several studies focused on the interaction between the pantograph and the catenary because it determines the quality of energy capture and therefore, the maximum reachable speed of train.

A new interest has born for portable systems able to assess pantographs health. The main task that the pantograph has to accomplish is to keep contact with the catenary wire, in the presence of disturbances, such as deflections, imposed by the line, train-roof-induced vibrations and aerodynamic forces. The interest is thus addressed so as to check the functionality of those elements influencing the dynamics of the mechanism i.e. the suspension systems.

In this paper, a simple strategy for the development of a vibration-based condition monitoring machine is introduced. The monitoring tool is meant to be as simple as possible, but able to judge in real-time the health of the suspensions, just requiring the train is at rest and isolated from the electrical line. The portability is an important customer requirement that limits weight; the set-up should need only a clamping to the pantograph frame. The machine will be equipped with a one DOF mechanism that excites the pantograph under inspection; accelerometers will collect the vibrating responses and the processing unit will elaborate a judgment on the overall dynamical behavior.

Analytical model that best fits the need is necessary because faults database is not available. The main assumption is that a two DOF system is accurate enough to describe the dynamics in the frequency range 0-10 Hz. Dynamical parameters are estimated by means of Lagrange's equations for any configuration in the working interval. To verify the assumption, a numerical modal analysis has been performed on a FEM model. Simulation results have been used to further considerations about the detection of structural defects. Phase plots are considered to be an interesting instrument to smartly recognize severe defects. As an example, a leakage in the dashpot was supposed; a significant deviation in the phase plots showed the suitability of the method.

G. Santamato, M. Solazzi, A. Frisoli are with PERCRO Laboratory, Scuola Superiore Sant'Anna, Pisa, Italy (e-mail: g.santamato@sssup.it, m.solazzi@sssup.it, a.frisoli@sssup.it).

II. Literature Review

A. Current Techniques for Vibration Based-Condition Monitoring

Vibration based structural health is one of the possible techniques available for condition monitoring. The system is excited by a testing input or directly by the environmental load for large-scale applications, i.e. bridges, building, and so on.

The exhibited vibrations are measured and elaborated in order to assess the health of the specimen, on the basis of alterations in the dynamical characteristics. A basic hypothesis should therefore be verified before applying this technique: the measured response is significantly altered once damage has occurred [1]. The main issue is the establishment of which vibrating index is mostly dependent on the effects of defects. The choice is even complicated because it depends upon boundaries conditions, different from one case to another; a parameter fit for a specific situation might instead reveal to be highly sensitive to measurement noise and modeling errors due to the environmental changes [2].

1. Frequency Analysis

The first and most commonly used strategies belong to the so called frequency-domain; they look for modifications in the modal parameters, i.e. frequencies and mode shapes. The basic

principle is that common defects like cracks alter properties as stiffness, mass, dissipation of energy; those modifications may be detected by a frequency-shift. In general, easy and reliable measurements can be conducted at a few points. However, frequency does not contain spatial information about the incipient damage as written in [3] and [1]. Some studies about bridge beams, [4], [5], witnessed that even alteration of the 90% in the stiffness of the cross sectional area, was not detectable from the shift.

2. Modal Shapes

Modal shapes alterations take into account spatial information, giving the chance to localize the affected regions. Previous studies affirm that eigenvectors are also more sensitive to damages [3]. On the other hand, to detect local-structural damages, it is necessary to investigate the high frequency band of the system under inspection. The good deal with the high frequency band concerns the required robustness of the investigator tool which must be able to excite the structure without deformations. To reconstruct local modes, it is required more number of sensors, which increases the cost and the time of the measurement.

3. Mode-Shape Related Methods

Coordinate Modal Assurance Criterion (COMAC), curvature and flexibility methods are evolved versions of the mode-shape related strategy. They are supposed to be more sensitive to loss of stiffness, but they need even more points to make the estimation reliable. Reference [6] presents experimental results applied on a full-size composite helicopter main rotor blade. The damage detection methods used in this study are COMAC and the modal strain energy method. The undamaged blade has been identified with the Experimental Modal Analysis and damage was simulated attaching a small mass to the blade. Both the methodologies were able to detect the location of defects. COMAC results were less sensitive than the strain energy technique, and the damage index did not detect the exact location of the added mass. The modal strain energy formulation provided good detection possibilities and sensitivity, even after hard calculations, necessary to estimate the damage index.

4. Novel Strategies of Vibration Based Condition Monitoring

Innovative strategies emerged in recent years to accomplish detection of complex phenomena or efficient systems for the real-time condition monitoring.

Some literature makes refer to nonlinear identification; [7] discusses the experimental nonlinear identification applied to an aircraft with bolted connections. Nonlinear methods rely on the assumption that due to damage the system might exhibit a nonlinear response even excited in a range in which its behavior was assumed to be linear.

Reference [8] proposes changes in the topology of the phase space as a clue of current damage. The research has been focused on a demonstrative case, focused on an arc, affected by radial cracks. Both numerical and experimental results demonstrate that the deviation of the phase space is more sensitive to damage and less sensitive to noise, than modal-based parameters.

B. Survey of Railway Pantographs Models

The literature contains several models of pantograph utilized in the analysis of the interaction with the catenary. An important issue concerns the choice of a proper model of pantograph. It seems that the general assumption is that pantograph global-rigid-body modes are not supposed to be influenced from the structural elasticity and damping, i.e. in the operating condition links may be considered as rigid bodies, but it is hard to find demonstration about this hypothesis. The literature agrees about the fact that the lumped or low-order models work up to 20 Hz [9]. With this hypothesis, it is possible to classify and locate the vibrating modes in the frequency domain, distinguishing a low frequency band in which are located the suspensions modes and a high frequency band, collecting combined effects of suspensions and structural dynamics. Lumped models differ on the base of the specific purpose of the study.

Another general hypothesis is that under the applied load the mechanism layout varies in the neighborhood of the initial operational point, so that a linear model is adopted [9]. References [10]-[12] make use of a two DOF system, while [13] introduces a three DOF system. Reference [14] increases the order by one, in order to model the pitch.

Reference [15] uses a four-rigid body model in a multi-body analysis, including the pan head, the plunger and the lower and upper arms, while in [16] is shown a comparison between a lumped model and a FEM model to simulate the exchanged force between the pantograph and the catenary, affirming that the simplified model is suitable.

III. Description of the Railway Pantograph

The railway pantograph under consideration, shown in Fig. 1, belongs to the so called symmetric scheme, because of the geometry in the transversal plane with respect to the motion of the train.

The tridimensional frame is made up of two parallelograms constrained by a couple of diagonal links such that the mechanism has one DOF which can be represented by the angle ϑ in the longitudinal plane, as depicted in Fig. 2. Each one of the four lower links is constrained to a corresponding shaft which can rotate around the y axis. The rotation of the motorized shaft is applied to the conducted one by means of two tie-rods. The mechanism is actuated by a pneumatic cylinder; when the cylinder is feed with compressed air, the piston moves up and drags the parallel springs, thus generating the rotation of the motorized shaft; the result is the lifting of the entire pantograph. A torsion bar prevents the eventual relative rotation between the parallelograms around the z axis.

The contact between the strip and the catenary wire is governed by two suspensions: the principal one (Fig. 3) is involved in the range of low frequency displacements (about 1.5 m), while the upper suspension (Fig. 4) compensates displacements at high frequencies between the pan head and the catenary. The springs which transmit the motion to the

motorized shaft furnish elasticity to the principal suspension. Damping is produced in three pneumatic dashpots, even though the black ones in Fig. 3 are meant to work only in the opening and closure modes. The secondary suspension is realized by the two springs connected on the top to the pan head.

Fig. 1 A picture of the railway pantograph under consideration (courtesy of Trenitalia)

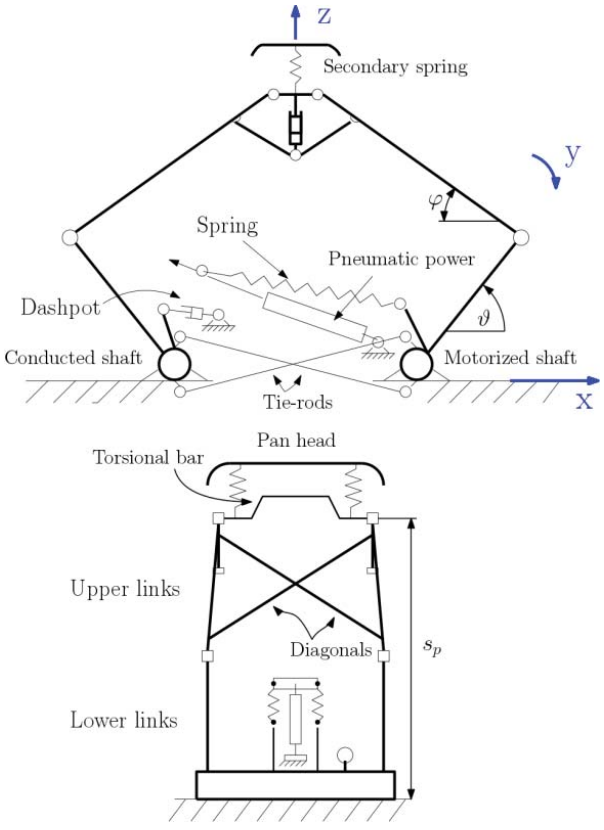

Fig. 2 Pantograph scheme

For all elements except for the torsional bar material is assumed to be structural steel with Young's modulus E equal to 210 GPa, density ρ equal to 7850 kg/m^3, Poisson's ratio v equal to 0.3; the torsional bar is in aluminum with Young's modulus E equal to 69 GPa, density ρ equal to 2700 kg/m^3, Poisson's ratio v equal to 0.3.

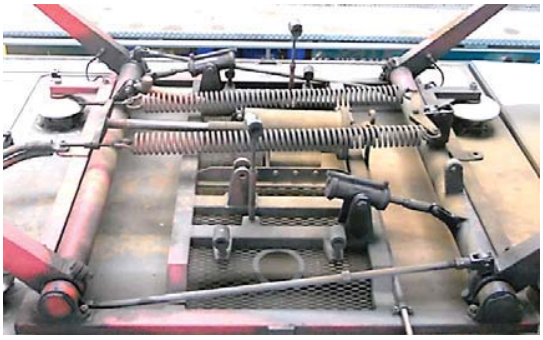

Fig. 3 Principal suspension (courtesy of Trenitalia)

Fig. 4 Secondary suspension and suspended pan head (courtesy of Trenitalia)

IV. Derivation of an Analytical Model of the Railway Pantograph

The identification of damages is meant to detect defects in the vertical oscillations. To simulate the effects of forecast damages, a model of the pantograph is necessary.

In this paper, we want to verify that structural elasticity does not influence the vertical oscillations of the pantograph, as well to estimate the lumped parameters. To reach the goal two distinct models have been built.

The first one is a two DOF lumped parameter model, whose scheme is depicted in Fig. 5; it has been derived considering links as rigid bodies, so by means of analytical dynamics laws, we have brought out an equivalent system.

The second model is a more accurate one and was obtained with the FEM, including all the relevant elements, and so considering distributed masses and elasticity. A comparison of results between the two models was accomplished to compare the predictive behavior of the first simplified model vs. the second FEM more accurate one.

Numerical test was conducted starting from an equilibrium position in the working space of the pantograph (correspondent to the interval ϑ_{min}-ϑ_{max} in Table I), with the assumption of small displacements, even though the kinematics is actually nonlinear. Linearity is extended to all the elements, including springs and dashpot; the last one, in particular, is modeled as a viscous damper with a constant damping coefficient. The chosen configuration is obtained when ϑ is equal to 59 deg. Table I collects the main geometrical and physical properties (M_{tot} stands for the total mass).

For the sake of simplicity, we will neglect deviations in dimensional and geometrical tolerances, considering that external and inner constraints i) act like ideal hinges deleting five DOF; ii) introduce negligible friction.

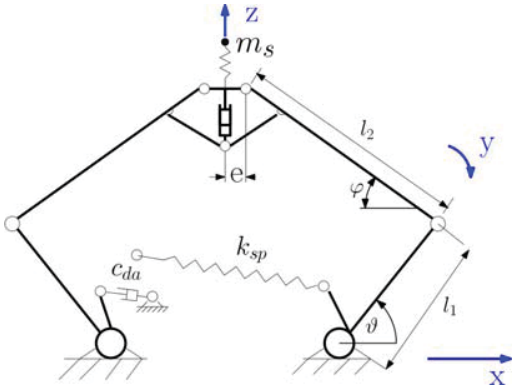

Fig. 5 Geometrical scheme of the pantograph

TABLE I
MAIN PROPERTIES OF THE PANTOGRAPH

Symbol	Value	Units
ϑmin	10	*deg*
ϑmax	59	*deg*
$s_{p,min}$	0.1179	*m*
$s_{p,max}$	2.167	*m*
l_1	1.100	*m*
l_2	1.659	*m*
e	0.045	*m*
M_{tot}	88.1570	*kg*
k_{sp}	9235.6	*N/m*
k_s	1621	*N/m*
c_{da}	6944.4	*N s/m*

A. Lagrange Formulation of the Pantograph Dynamics

Under the previous assumptions, we can use Lagrangian mechanics. Pantograph motion is planar with respect to the *x*-*z* plane; there is also a symmetry with respect to the *z*; thus we obtain an eccentric crank-rod scheme as shown in Fig. 6.

Ω is the origin of the Cartesian axes. The crank 1 represents one of the lower arms on the right in Fig. 2; the rod 2 represents the upper arms and the diagonal on the right in Fig. 2; the slider element 3 represents the torsion bar. G_1 is the crank center of mass; r_1 is the distance between G_1 and the hinge in Fig. 6; G_2 is the rod center of mass. The crank-rod mechanism is reduced to a system of punctual masses and concentrated moments of inertia, shown with points and rings in Fig. 7.

The following legend needs to be considered: m_1 is the mass of the crank; J_1 is the moment of inertia of the crank with respect to its center of mass; J_A is the half moment of inertia along the *y* axis of the shafts, the tie-rods, the springs and the dashpot, evaluated with respect to point A. Because the rod rotates around a moving instantaneous center of rotation, it is easier to use a fictitious system with the same mass m_2 and the same kinetic energy; from the equivalence we obtain two masses m_B and m_C located at the extremes and a moment of inertia J_{BC} around the center of mass. Table II collects the values.

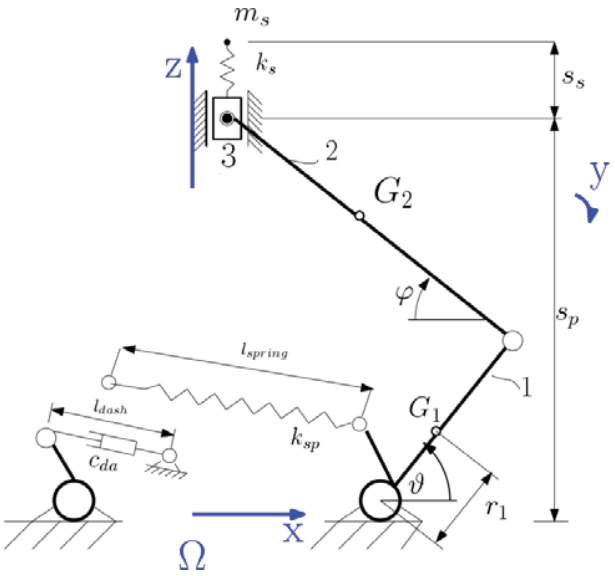

Fig. 6 Equivalent kinematic scheme

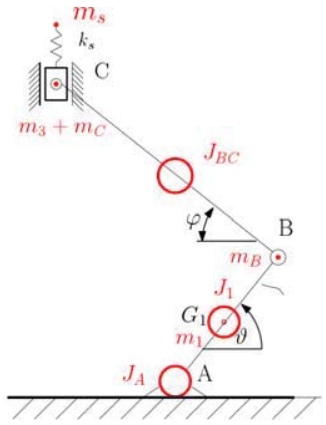

Fig. 7 Reduction of the mechanism to a system of punctual masses and moments of inertia

TABLE II
VALUES OF MASSES AND INERTIAS OF THE REDUCED MECHANISM

Symbol	Value	Units
m_1	1.6775	*kg*
m_2	2.7029	*kg*
m_B	1.4074	*kg*
m_C	1.2955	*kg*
m_3	2.3101	*kg*
m_s	15	*kg*
J_A	-0.9110	*kg m²*
J_1	0.1413	*kg m²*
J_{BC}	-1.2682	*kg m²*

Since we aim at reducing the dynamics to the *z* axis, s_p and s_s are assumed as Lagrangian parameters; ϑ and φ are assumed as normal coordinates locating the crank and the rod position with respect to any slider coordinate.

For the kinetic energy T, if T_p is the contribution due to the pantograph and T_s to the suspended mass, the following expression holds:

$$T_p = \frac{1}{2}\left[\left(2\cdot J_A + 4\cdot J_1 + 4\cdot m_1 r_1^{\,2} + 2\cdot m_B l_1^{\,2}\right)k_\vartheta^{\,2} + \right. \\ \left. +2\cdot J_{BC}k_\varphi^{\,2} + 2\cdot m_C + m_3\right]\dot{s}_p^{\,2}; \quad (1)$$

$$T_s = \frac{1}{2}m_s\dot{s}_s^{\,2}; \quad (2)$$

$$T = T_p + T_s; \quad (3)$$

where;

$$k_\vartheta = \frac{d\vartheta(s)}{s}; \quad (4)$$

$$k_\varphi = \frac{d\varphi(s)}{s}; \quad (5)$$

From the (1), it is possible to define an equivalent mass m_p varying with s_p, as follows:

$$m_p\left(s_p\right) = \left(2\cdot J_A + 4\cdot J_1 + 4\cdot m_1 r_1^{\,2} + 2\cdot m_B l_1^{\,2}\right)k_\vartheta^{\,2} + \\ +2\cdot J_{BC}k_\varphi^{\,2} + 2\cdot m_C + m_3; \quad (6)$$

Fig. 8 illustrates the dependence of the equivalent parameter in the working range of s_p; as s_p increases, the inertia of the mechanism gets higher because the corresponding rotation of the links decreases.

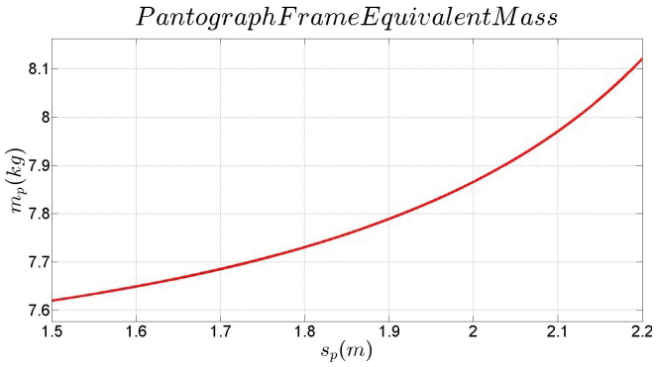

Fig. 8 Pantograph frame equivalent mass

For the potential energy U, we have U_p for the pantograph and U_s for the suspended mass. So:

$$U = U_p + U_s \quad (7)$$

$$U_p = \frac{1}{2}\left(2\cdot k_{sp}\right)\left(\frac{dl_{spring}}{ds_p}\right)^2 s_p^{\,2} \quad (8)$$

$$U_s = \frac{1}{2}k_s\left(s_s - s_p\right)^2 \quad (9)$$

It is thus possible to define an equivalent stiffness k_p varying with s_p, as:

$$k_p\left(s_p\right) = 2\cdot k_{sp}\left(\frac{dl_{spring}}{ds_p}\right)^2; \quad (10)$$

Fig. 9 illustrates the dependence of the equivalent parameter in the working range of s_p; while s_p increases, k_p does the same.

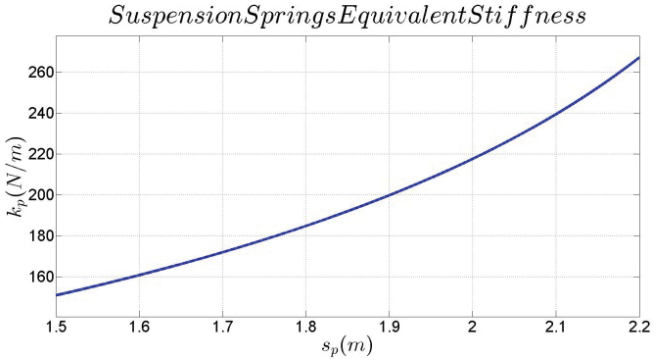

Fig. 9 Suspension springs equivalent stiffness

Viscous damping force is accounted for the Rayleigh's dissipation function F [17]:

$$F = \frac{1}{2}c_{da}k_d^{\,2}\dot{s}_p^{\,2}; \quad (11)$$

where

$$k_d = \frac{dl_{dash}}{ds} \quad (12)$$

Fig. 10 illustrates the dependence of the equivalent parameter in the working range of s_p; while s_p increases, c_p does the same.

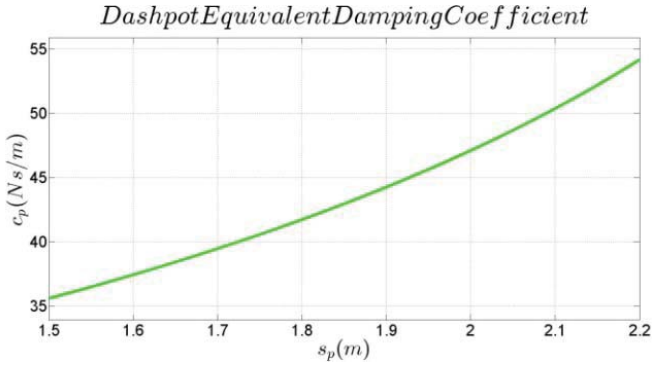

Fig. 10 Dashpot equivalent damping coefficient

Lagrange's equations for the unforced system can be written as follows:

$$\begin{cases} \dfrac{d}{dt}\left(\dfrac{\partial T}{\partial \dot{s}_p}\right)-\dfrac{\partial T}{\partial s_p}+\dfrac{\partial U}{\partial s_p}+\dfrac{\partial F}{\partial \dot{s}_p}=0; \\ \dfrac{d}{dt}\left(\dfrac{\partial T}{\partial \dot{s}_s}\right)-\dfrac{\partial T}{\partial s_s}+\dfrac{\partial U}{\partial s_s}+\dfrac{\partial F}{\partial \dot{s}_s}=0; \end{cases} \tag{13}$$

By substituting the previous definitions and neglecting the kinetic energy derivatives with respect to the Lagrangian coordinates [17], one obtains:

$$\begin{cases} m_p\left(s_p\right)\ddot{s}_p+c_p\left(s_p\right)\dot{s}_p+k_p\left(s_p\right)\left(s_p-s_s\right)=0; \\ m_s\ddot{s}_s+k_s\left(s_s-s_p\right)=0; \end{cases} \tag{14}$$

The pantograph mechanism can be thus reduced to a two DOF model with lumped parameters dependent on the Lagrangian coordinate s_P (see Fig. 11).

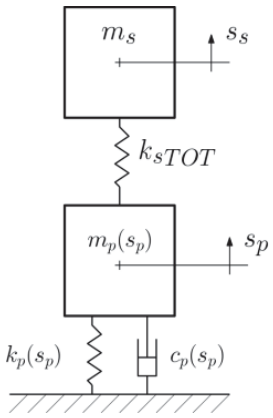

Fig. 11 Lumped model

For the pantograph frame, in particular, it is possible to define a natural frequency f_n as well as a damping factor ξ and a damped natural frequency f_d per each value of s_p as follows:

$$f_n\left(s_p\right)=\sqrt{\frac{k_p\left(s_p\right)}{m_p\left(s_p\right)}}; \tag{15}$$

$$\xi\left(s_p\right)=\frac{c_p\left(s_p\right)}{2\sqrt{m_p\left(s_p\right)k_p\left(s_p\right)}}; \tag{16}$$

$$f_d\left(s_p\right)=f_n\left(s_p\right)\sqrt{1-\xi\left(s_p\right)^2}; \tag{17}$$

It is interesting to notice, in Fig. 12, that despite both m_{eq} and k_{eq} increase with s_p, the natural frequency increases as well, meaning that the dependence of k_{eq} from s_p is more important than that of m_{eq}. The damped frequency follows the same pattern.

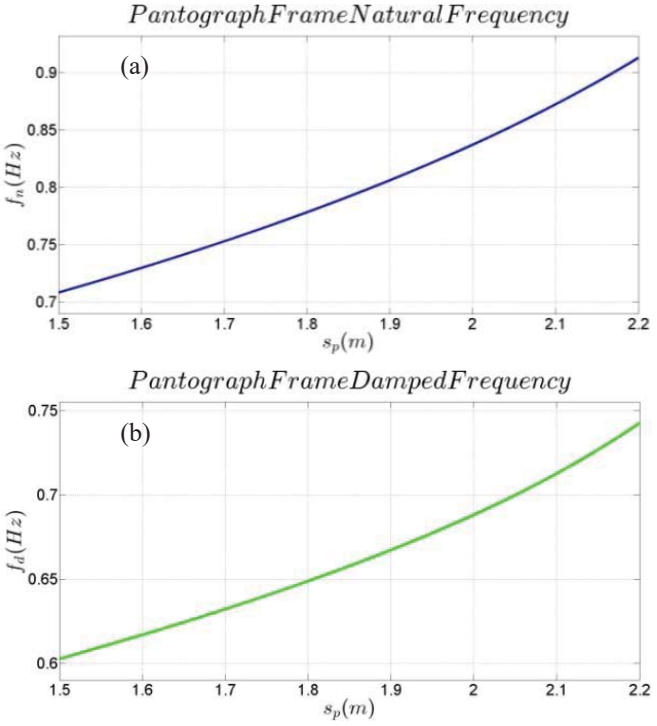

Fig. 12 Pantograph frame natural (a) and damped frequency (b)

The linearized equations about the equilibrium position of interest, at s_p=2.166 m may be written in the matrix form:

$$\underline{\underline{M}}\,\underline{\ddot{q}}(t)+\underline{\underline{C}}\,\underline{\dot{q}}(t)+\underline{\underline{K}}\,\underline{q}(t)=\underline{0} \tag{18}$$

where;

$$\underline{q}=\begin{pmatrix} s_p \\ s_s \end{pmatrix}; \tag{19}$$

$$\underline{\underline{M}}=\begin{pmatrix} m_p & 0 \\ 0 & m_s \end{pmatrix} \tag{20}$$

$$\underline{\underline{C}}=\begin{pmatrix} c_p & 0 \\ 0 & 0 \end{pmatrix} \tag{21}$$

$$\underline{\underline{K}}=\begin{pmatrix} k_p & 0 \\ 0 & k_p+k_{s_{TOT}} \end{pmatrix} \tag{22}$$

Table III collects the values for the configuration under consideration.

The system is subjected to arbitrary viscous damping, because the damping matrix $\underline{\underline{C}}$ is not proportional to the mass matrix $\underline{\underline{M}}$ and the stiffness matrix $\underline{\underline{K}}$; for this reason, the calculation of the damped frequencies is not possible in the configuration space; however it is possible to use the state space. To this end, we introduce the state space vector $\underline{x}$ as:

$$\underline{x} = \begin{Bmatrix} \underline{q} \\ \underline{\dot{q}} \end{Bmatrix}. \tag{23}$$

We can rewrite the (18) in the customary state form:

$$\underline{\dot{x}}(t) = \underline{\underline{A}}\,\underline{x}(t) \tag{24}$$

where;

$$\underline{\underline{A}} = \begin{bmatrix} \underline{\underline{0}} & \underline{\underline{I}} \\ -\underline{\underline{M}}\,\underline{\underline{K}} & -\underline{\underline{M}}\,\underline{\underline{C}} \end{bmatrix} \tag{25}$$

where $\underline{\underline{0}}$ is the *2x2* null matrix and $\underline{\underline{I}}$ is the *2x2* identity matrix. The modal frequencies can be carried out from the two couples of poles of $\underline{\underline{A}}$ [17]. Natural frequencies $(f_n)_i$ are equal to the magnitude of poles under 2π, while the damped frequencies $(f_d)_i$ correspond to the imaginary part of poles under 2π. To better underline the effect of damping, modal damping ratios ξ_i are also evaluated, as in:

$$\xi_i = \sqrt{\left(1 - \left(\frac{(f_d)_i}{(f_n)_i}\right)^2\right)}. \tag{26}$$

Table IV collects the obtained values (*i* stands for the imaginary unit).

TABLE III
LUMPED PARAMETERS OF THE EQUIVALENT 2 DOF

Symbol	Value	Units
s_p	2.166	*m*
m_p	8.0621	*kg*
m_s	15	*kg*
k_p	256.99	*N/m*
k_{sTOT}	3242	*N/m*
c_p	52.81	*N·s/m*

TABLE IV
CALCULATED SCALAR MODAL PARAMETERS OF THE 2 DOF SYSTEM

Poles	Natural frequency (Hz)	Damping ratio (/)	Damped frequency (Hz)
-1.0862 ± 3.1236i	0.5263	0.3284	0.4971
-2.1889 ± 24.9973i	3.9937	0.0872	3.9784

B. Development of FEM Model of the Pantograph

In order to verify the assumption discussed in Sec. A numerical modal analysis has been performed by means of the commercial software ANSYS. Structural elements have been modeled with thick beam elastic elements (BEAM 188 in ANSYS). The ratio between the length of the links and their cross sectional characteristic dimension is around 15%, so that Timoshenko's theory must be applied. Springs are modeled with longitudinal springs elements (COMBIN14) with three DOF per each node. To simulate the inertia of the pan head two concentrated masses with three DOF (MASS21) have been applied on the top of the upper springs.

The QRDAMP method is suitable because high damping ratio is expected to be present. The following Table V reports the first 20 natural and damped frequencies. Damping factors have relevant values only for the first two modal frequencies, but are negligible for all the others, so that the modes above 4 Hz are almost undamped. Frequencies lie in the 0-50 Hz range and it is possible to notice that some couples of modes have about the same frequency, as a result of the geometric symmetry of the pantograph.

TABLE V
ESTIMATED SCALAR MODAL PARAMETERS OF THE FEM MODEL

Frequency Number	Natural frequency (Hz)	Damping factor (/)	Complex Frequency (Hz)
1	0.5224	0.3108	0.5
2	3.8382	$0.7689 \cdot 10^{-1}$	3.8025
3	9.8369	$0.8951 \cdot 10^{-4}$	9.8369
4	13.4508	$0.3115 \cdot 10^{-2}$	13.4481
5	19.3517	$0.1766 \cdot 10^{-4}$	19.3517
6	21.7291	$0.3039 \cdot 10^{-2}$	21.7266
7	22.2107	$0.8126 \cdot 10^{-4}$	22.2104
8	23.0749	$0.2135 \cdot 10^{-3}$	23.0744
9	23.8704	$0.1809 \cdot 10^{-3}$	23.8701
10	26.4331	$0.2033 \cdot 10^{-3}$	26.4328
11	28.9848	$0.8505 \cdot 10^{-4}$	28.9847
12	30.4000	$0.9667 \cdot 10^{-6}$	30.3994
13	30.4000	$0.3724 \cdot 10^{-7}$	30.4000
14	31.6389	$0.7215 \cdot 10^{-3}$	31.6385
15	31.8897	$0.1656 \cdot 10^{-3}$	31.8890
16	34.8633	$0.3346 \cdot 10^{-3}$	34.8628
17	36.2361	$0.5148 \cdot 10^{-4}$	36.2361
18	37.2559	$0.7242 \cdot 10^{-4}$	37.2558
19	50.3291	$0.6885 \cdot 10^{-4}$	50.3290
20	51.1194	$0.5784 \cdot 10^{-4}$	51.1194

Figs. 13 and 15 show the real part of the eigenvectors, that is the natural mode shapes. From the observation of the first two mode shapes, in Fig. 13, it seems that no structural deformation appears.

Fig. 14 illustrates another mode present in the band of interest, associated to a bending around *x* axis. All the other modes, located at higher frequencies, may be considered local, because they exhibit deformations confined to restricted regions. Structural modes of the thinner beams appear in the modal set and according to this, modal density increases above the global-modes-band. The ratio between the cross-sectional moment of inertia and the geometrical length is really different between the main beams of the frame; for the diagonal the ratio is 1.3308 m^{-3}, while for the lower beam is 0.0764 m^{-3}; this proves that mainly the only upper arms vibrate and the lower arms are not involved because of their high stiffness with respect to the pantograph frame. In pictures (a), (b), (c), in Fig. 15 are evident different bending modes of the upper half of the frame. Mode shapes may be thereby classified as in Fig. 16.

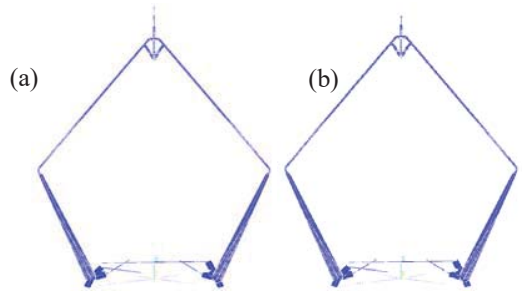

Fig. 13 (a) First mode shape (0.52 Hz); (b) Second mode shape (3.8025 Hz)

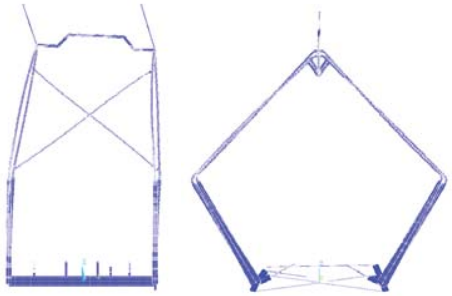

Fig. 14 Third mode shape (9.8369 Hz)

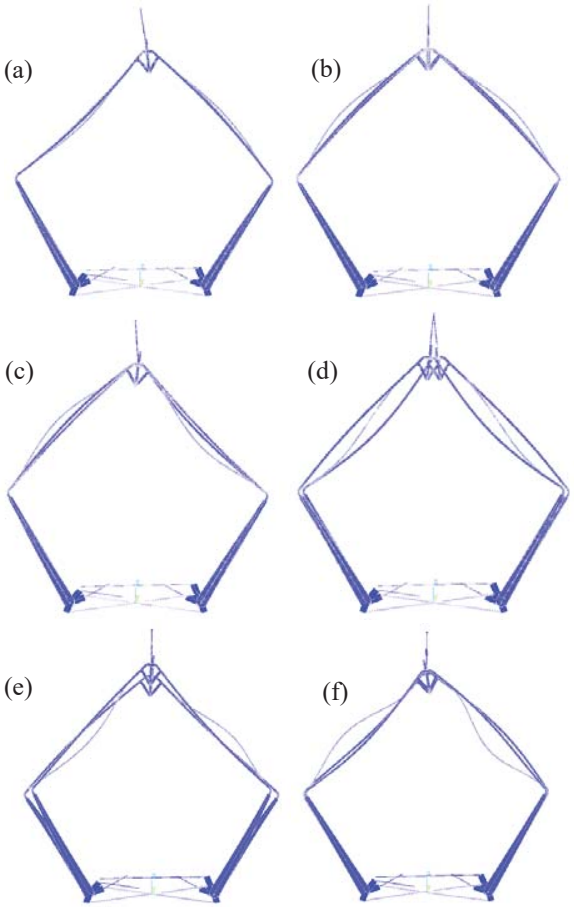

Fig. 15 Some mode shapes in the interval 0-50 Hz; (a) at 13.4481 Hz; (b) at 19.3517 Hz; (c) at 21.7266 Hz; (d) at 23.8701 Hz; (e) at 28.9847 Hz; (f) at 31.6385 Hz

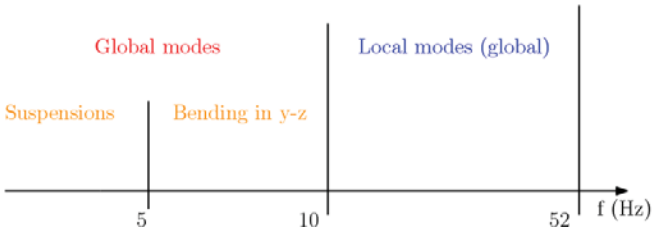

Fig. 16 Classification of estimated modes in the frequency range

C. Comparison of FEM vs analytical model

The following Table VI synthetizes the comparison between the estimation based on the modal frequencies. Considering the simplified model brings some error; in particular, the approximation is better on the first mode, as demonstrated by lower percentage errors on the natural frequency and damping ratio. Natural frequencies are better estimated than damping ratios for both modes.

Because the interest lies on the development of a strategy that detects deviations from the dynamic response, there is no need to reconstruct with extreme precision the dynamic properties. The assumption that the two DOF model is equivalent to the pantograph behavior is thus adequately demonstrated.

TABLE VI
COMPARISON BETWEEN THE ANALYTICAL MODEL AND THE FEM MODEL

Parameter	Analytical calculation	FEM estimation	Absolute percentage error
$(fn)_1$ (Hz)	0.5263	0.5224	0.7520
$(fn)_2$ (Hz)	3.9937	3.8382	4.0505
ξ_1 (/)	0.3284	0.3108	5.6758
ξ_2 (/)	0.0872	0.0769	13.4489

V. DAMAGE PREDICTION BY PHASE PLOTS ANALYSIS

A. Numerical Simulation of Damage in the Dashpot

In terms of appreciable defects, it is important to notice that local modes are associated with the high-frequency band, as shown from the numerical modal analysis. In order to excite the specimen without deformations, the required stiffness might be incompatible with the portability. Frequency techniques need also to record measurements in the neighborhood of all the regions supposed to suffer defects during their life. As a conclusion, it is hard to recognize defects like clearance in the hinges and cracks with a simple system. This is the reason that brings us to focus on faults prone to be detected in the easiest way, such as those affecting the low-frequency dynamics. The main idea of our analysis is to use deviations in the phase plot as an index of damage. This choice is particularly suitable in this case; detection, in fact, aims to recognize those alterations that significantly influence the shape of the phase plots.

Fault models are necessary to predict possible damages when historical data are not available. We simulated a leakage in the dashpot that yields to a reduction of the damping coefficient of 90%. Damped frequencies vary as reported in Table VII.

TABLE VII
VARIATION IN THE DAMPED FREQUENCIES DUE TO THE SIMULATED DAMAGE

Frequency (Hz)	Safe pantograph	Damaged pantograph	Absolute percentage deviation
$(f_d)_1$	0.4971	0.5221	5.0292
$(f_d)_2$	3.9784	4.0238	1.1412

The analysis simulates the free response of the system under an imposed initial displacement, applied on the pantograph frame DOF The intensity of the displacement has been chosen such that the assumption of linearity is satisfied; for example, a value of 0.02 m has been used; as a proof, the modification in natural frequencies and damping ratios produced by the considered displacement is less than 1%. The integration has been carried out so as the transient of the damaged system would be extinguished; the result is a time interval of 75 s.

The historical series are depicted for the first 8.5 s in Fig. 17.

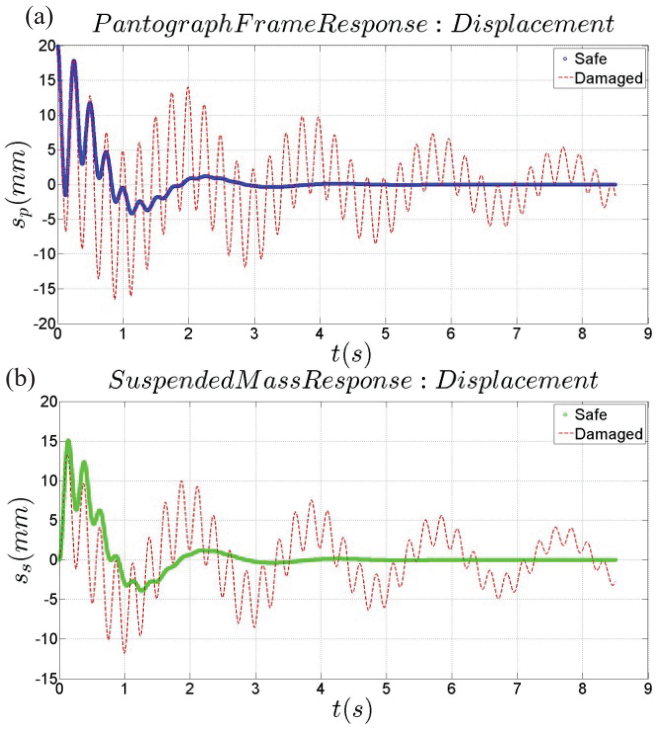

Fig. 17 Time histories (8.5 s); (a) pantograph frame; (b) suspended mass

From the time series, it is immediate to reconstruct the trajectories in the so called phase space, i.e. the phase plots. The phase plot is a parametric representation expressing the relationship between the components of the state-space vector of the system. The parameter is time, i.e. each point on the phase plot curve represents the values assumed by the state components in a certain instant of time. For the present case, the phase space is defined as in (23).

For an unforced system, dynamics is expressed by:

$$\begin{cases} \dot{\underline{x}} = F\left(\underline{x}\right); \\ \underline{x}\left(0\right) = \underline{x}_0; \end{cases} \tag{27}$$

As time increases, the state evolves, under the dynamic law F, starting from the initial condition $\underline{x}_0$. Phase plots are usually used to study the stability properties of a system. Starting from an equilibrium position or fixed-point, the response to small perturbations is different depending on the kind of system [17]. The most interesting aspect is that also the so-called *attractor* might change. The attractor is a subset of the phase space that may be thought of as a region to which all trajectories tend to as time goes to infinity [8]. For a damped oscillator, the attractor is the origin of the plane; after the perturbation the system describes a trajectory corresponding to a converging spiral. An undamped oscillator tends instead, to an elliptic curve, since the dynamic equilibrium is governed by the balance of inertia and elastic forces.

Fig. 18 reports the phase plots for a safe and a damaged pantograph; in pictures (a) and (b) safe and damaged structure solutions are overlapped, per each DOF. Patterns mismatch for both DOF solutions. To quantify the difference in trajectories, we can take as reference points those in which velocity is null, because they are easier to be identified, as shown in pictures (c), (d), (e), where they are labeled with alphabetic letters (*A-H* and α-θ for the continuous curve and *Ad-Hd* and α_d-θ_d for the dotted one). Point A represents the first time in which, after the initial displacement, velocity is null; in B the phenomenon happens for the second time and so on for the successive points. By analogy, we can define points *Ad-Fd* as well as α-θ and α_d-θ_d . The first step is to evaluate the distance between two consecutive reference points on the damaged structure phase plot, for several couples of points. The discrepancy with the corresponding distances for the safe pantograph is an eligible parameter to detect faults. Table VIII collects the values of distance for four couples of points. The relative percentage difference increases with the trajectories abscissa, (i.e. the time) and except for the first couple it is about 100%. The deviation takes into account the different amplitudes of the response, due to the variation in damping. We notice that reference points correspond, in the time history, to the peaks of the response.

Fig. 19 illustrates the phase plots for the last 25 s; in the case of damaged structure the system is still approaching the attractor, while for the safe pantograph the motion is expired as shown from the values of displacement and speed.

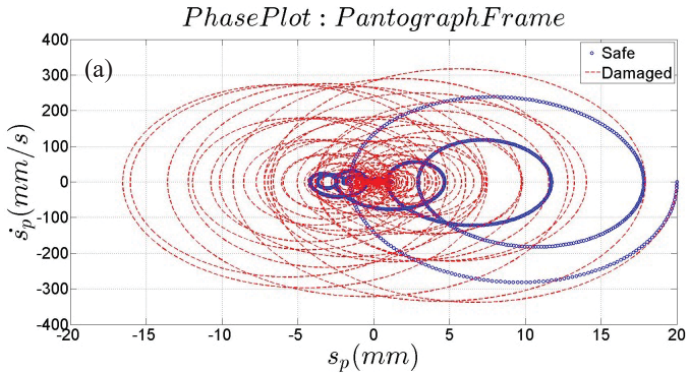

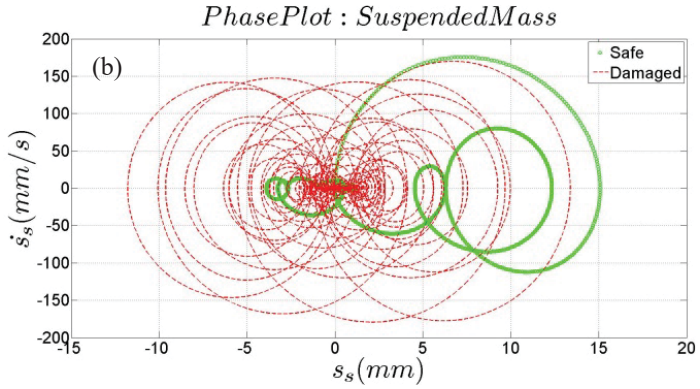

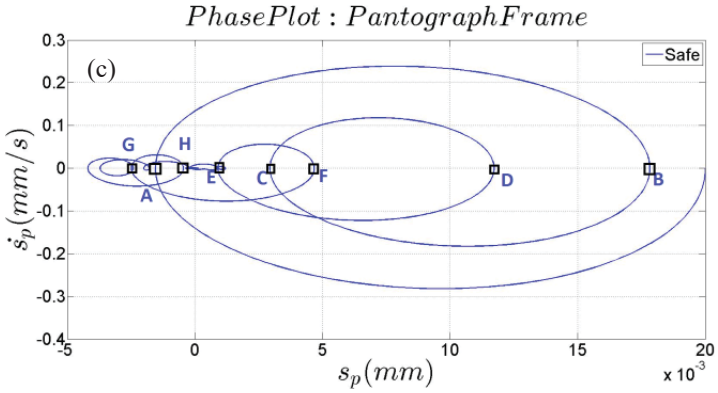

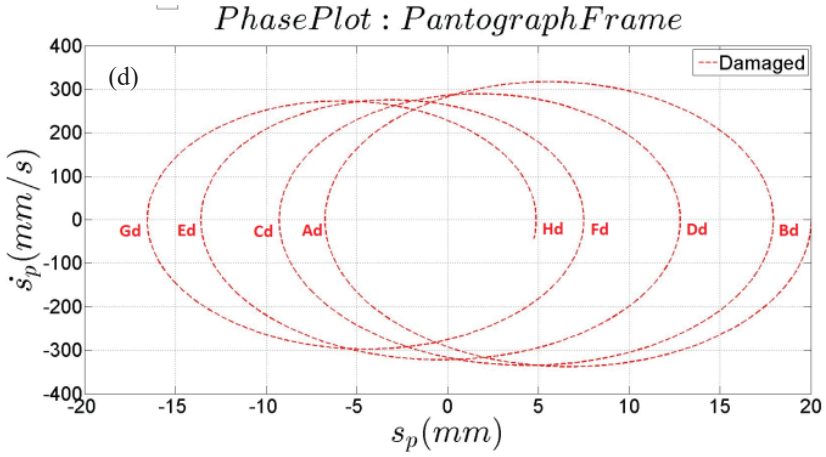

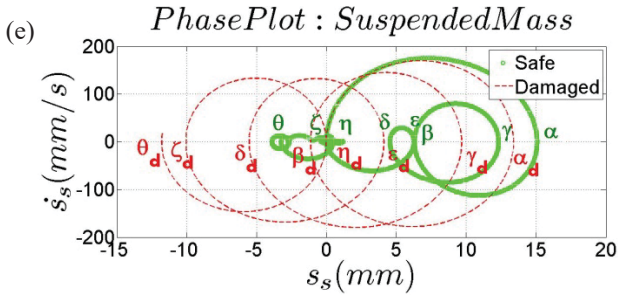

Fig. 18 Phase plots for the safe and damaged structure; (a) pantograph frame DOF; (b) suspended mass DOF; useful portions of trajectories obtained for the pantograph frame DOF: (c) safe structure; (d) damaged structure; (e) useful portions of trajectories obtained for the suspended mass DOF

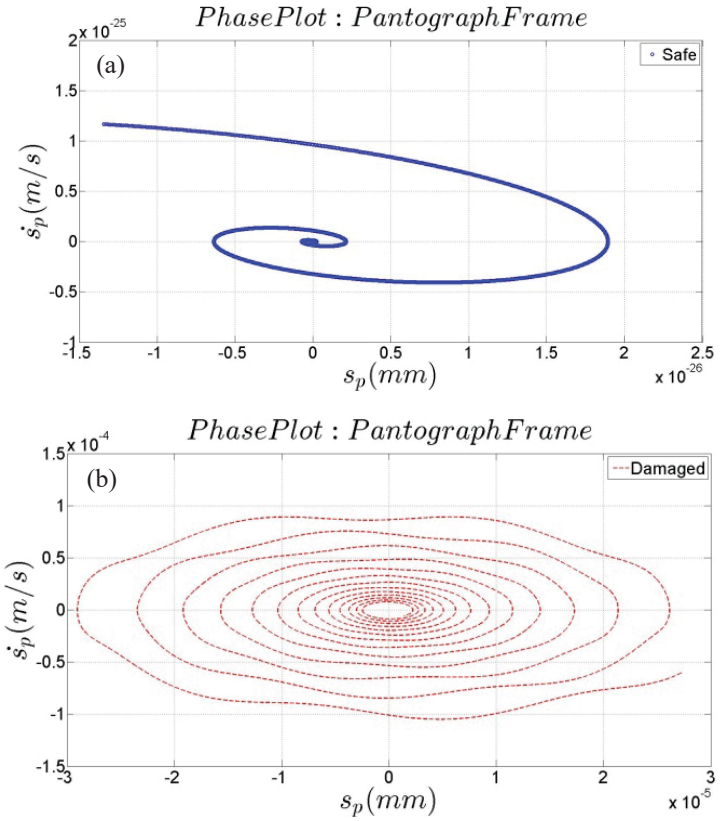

Fig. 19 Pantograph frame DOF trajectories approaching attractors; (a) safe structure; (b) damaged structure

TABLE VIII
PHASE PLOTS DISCREPANCY

Distance for safe pantograph	Distance for damaged pantograph	Absolute percentage deviation
A-B=19.3720	A_d-B_d = 24.6700	27.3488
C-D=8.770	C_d-D_d=21.3510	143.4550
E-F=3.7634	E_d-F_d=21.0620	459.6535
G-H=2.0359	G_d-H_d=24.4080	1098.9
α-β=8.7840	α_d-β_d=14.5040	65.1184
γ-δ=7.7960	γ_d-δ_d=15.1990	94.9590
ε-ζ=6.2976	ε_d-ζ_d=14.1720	125.0374
η-θ=3.7316	η_d-θ_d=11.7626	215.2160

B. Final Considerations

The convenience in the use of phase plots is that the detection strategy may be transformed in a simple problem of pattern recognition. It is not necessary to estimate with high precision the properties of the systems; it is only required to recognize a difference between the trajectories obtained from the specimen and those of the safe structure.

For the simulated fault frequency shift is about 5% on the first frequency; it is even lower on the second one. With the use of phase plots, several values of the discrepancy index may be obtained. In the proposed simulation, the four values are in the interval 30-1000%. It is clear that in this analysis the use of phase plots is more effective than the frequency technique.

From a practical point of view, a detection strategy that makes use of time measurements is simpler than a frequency-based one. The necessary Experimental Modal Analysis demands, in fact, for more computational effort in order to estimate modal parameters.

VI. Conclusions

Detection systems able to recognize incurring damages are powerful instruments to guarantee the functionality of structures as well to reduce cost of maintenance.

In this paper, we deal with the elaboration of a strategy for the detection of faults in railway pantographs. The research is constrained by specific customer requirements such as portability and ease in use, so the analysis is focused on the main dynamics of the pantograph, rather than on each element prone to failure.

The development of the strategy needs a model of pantograph because no historical data on damages are available. A simplified model has been obtained by means of analytical dynamics. The assumptions have been verified comparing modal frequencies calculated from the analytical model with those evaluated by a complete FEM model. The difference in results is acceptable, for the purpose of the analysis, so the lumped model is verified.

The use of phase plots for the detection of faults seems to be a convenient choice with respect to the requirements of portability and simplicity; it is in fact immediate to construct the trajectories, once time histories are known. The leakage in the dashpot has been simulated, by reducing the associated damping coefficient. The proposed strategy compares the shape of phase plots prior and after the damage. The noticed discrepancy is evident and more appreciable than frequency shift.

In a next step, the model will be validated by an Experimental Modal Analysis. Further studies are needed to take into account the effects of nonlinearities on phase trajectories; tests are also required to prove the suitability of the method.

Acknowledgment

The authors would like to thank *Trenitalia Spa* for the support given during the development of the research activities.

References

[1] Farrar and S. Doebling, "Damage detection II: field applications to large structures," in Modal Analysis and Testing, Kluwer Academic Publishers, 1999.

[2] B. Peeters, G. Lowet, H. Van der Auweraer and J. Leuridan, "A new procedure for modal parameters estimation," LMS International, Leuven, 2004.

[3] P. E. Carden and P. Fanning, "Vibration based condition monitoring: a review," Structural Health Monitoring, Vols. 3-(4), pp. 355-377, December 2004.

[4] C. R. Farrar, W. E. Baker, T. M. Bell, K. M. Cone, T. W. Darling, T. A. Duffey, A. Eklund and A. Migliori, "Dynamic characterization and damage detection in the I-40 bridge over the Rio Grande Los Alamos National Laboratory Report LA-12767-MS," Los Alamos Laboratory, Los Alamos, 1994.

[5] Z. Y. Shi, S. S. Law and L. M. Zhang, "Structural damage detection from modal strain energy change," Journal of Sound and Vibration, Vols. 218-(5), pp. 825-844, 1998.

[6] F. L. M. dos Santos, B. Peeters, H. Van der Auweraer, L. C. S. Goes and W. Desmet, "Vibration-based damage detection for a composite helicopter main rotor blade," Case Studies in Mechanical Systems and Signal Processing, p. 2016, submitted.

[7] G. De Filippis, J. P. Noel, G. Kerschen, L. Soria and C. Stephan, "Experimental nonlinear identification of an aircraft with bolted conncections," in Proceedings of the International Modal Analysis Conference (IMAC) XXXIII, Orlando, 2015.

[8] N. Zhenhua, H. Hong and M. Hongwei, "Using vibration phase space topology changes for structural damage detection," Structural Health Monitoring, vol. 11 (5), p. 538–557, 2012.

[9] G. Poetsch, J. Evans, R. Meisinger, W. Kortum, W. Baldauf, A. Veitl and et al., "Pantograph/catenary dynamics and control," Vehicle System Dynamics, pp. 159-195, 1997.

[10] A. Matvejevs and A. Matvejevs, "Pantograph-catenary system modeling using MATLAB-Simulink algorithms," Scientific Journal of Riga Technical University, 2010.

[11] D. Ritzberger, E. Talic and A. Schirrer, "Efficient simulation of railway pantograph /catenary interaction using pantograph-fixed coordinates," International Federation of Automatic Control, Vols. 48-1, pp. 61-66, 2015.

[12] J. Benet, A. Alberto, E. Arias and T. Rojo, "A Mathematical Model of the pantograph-catenary dynamic interaction with several contact wires," International Journal of Applied Mathematics, Vols. 37-(2), 2010.

[13] A. Alberto, J. Benet, E. Arias, D. Cebrian, T. Rojo and F. Cuartero, "A high performance tool for the simulation of the dynamic pantograph–catenary interaction," Mathematics and Computers in Simulation, vol. 79, pp. 652-667, 2008.

[14] A. Kumaniecka and M. Prącik, "Journal of theoretical and applied mechanics," Modelling and identification of catenary-pantograph system, Vols. 41-(4), pp. 887-901, 2003.

[15] J.-H. Seo and H. Sugiyama, "Three-dimensional large deformation analysis of the multibody pantograph/catenary systems," Nonlinear Dynamics, vol. 42, pp. 199-215, 2005.

[16] J. R. Jimenez-Octavio, M. Such, A. Carnicero and Lopez-Garcia, "Validation of simulation approaches for catenary-pantograph dynamics," in Ninth International Conference on Computational Structures Technology, Stirlingshire, 2008.

[17] L. Meirovitch, Fundamentals of Vibrations, Waveland Press, Inc., 21-44; 273-276;345-355.

Giancarlo Santamato (Eng., MSc) since January 2016, is research fellow at Scuola Superiore di Studi Universitari e Perfezionamento Sant'Anna in Pisa, Italy. His research interests concern: mechanics of vibrating systems, kinematics and dynamics of mechanisms and development of robotic tools for condition monitoring.

Massimiliano Solazzi (Eng., PhD) since August 2011, is Assistant Professor in Applied Mechanics at Scuola Superiore di Studi Universitari e Perfezionamento Sant'Anna in Pisa, Italy. His research interests concern: the design of robotic interfaces for virtual reality, teleoperation and rehabilitation assisted by robots, the design and control of arm exoskeletons, the development of control systems for manipulators, and the psychophysical validation of human machine interfaces. Massimiliano Solazzi has collaborated in numerous research projects both nationally and internationally. Currently he is carrying out research activities within the EU projects "Beaming","VERE", and "WearHap".

Antonio Frisoli (Eng., PhD) is Associate Professor of Robotics at Scuola Superiore Sant'Anna, where he is currently head of the Human-Robot Interaction area at PERCRO laboratory of TeCIP. He received his PhD (2002) with honors in Industrial and Information Engineering from Scuola Superiore Sant'Anna, Italy and the MSc (1998) in Mechanical Engineering, minor Robotics, from University of Pisa, Italy. He covers numerous positions as Associate Editors in major haptics and robotics IEEE conferences; he has been the former chair of the IEEE Technical Committee on Haptics, responsible for IEEE Robotics & Automation Society of the CEMRA Educational Program on Haptics and he is Associate Editor for Presence MIT Press and IEEE Robotics and Automation Letters. Antonio Frisoli's research interests are in the field on advanced kinematics, design and control of haptic devices and robotic systems, rehabilitation robotics and human motor control, virtual reality, advanced human computer interfaces for training, Brain Computer Interfaces. Currently he is studying new designs for exoskeletons systems, portable fingertip haptics and new brain-robot interfaces. He is author of more than 200 papers in peer-reviewed international conferences and scientific journals.